A Root-Locus Design Methodology Derived from the Impedance Stability Criterion and Its Application for LCL Grid-Connected Converters

Diaz, Enrique Rodriguez; Freijedo Fernandez, Francisco Daniel; Golsorkhi, Mohammad; Quintero, Juan Carlos Vasquez; Guerrero, Josep M.

Published in:
Proceedings of 18th European Conference on Power Electronics and Applications (EPE'16 ECCE Europe), 2016

DOI (link to publication from Publisher):
10.1109/EPE.2016.7695473

Publication date:
2016

Document Version
Early version, also known as pre-print

A Root-Locus Design Methodology Derived from the Impedance Stability Criterion and Its Application for LCL Grid-Connected Converters

Enrique Rodriguez-Diaz, Francisco D. Freijedo, Mohammad S. Golsorkhi
Juan C. Vasquez and Josep M. Guerrero
www.microgrids.et.aau.dk

Keywords

≪Ac/dc converter≫, ≪Active damping≫, ≪Converter control≫, ≪Wind energy≫.

Abstract

This paper presents a systematic methodology for design and tuning of the controller of LCL grid-connected converters. The proposed approach is derived from the impedance/admittance stability formulation, which eases the controller modelling of LCL grid-connected systems. After system modelling, a modified sensitivity function is defined to analyze the closed loop dynamics. For practical development, the control objectives are linked to main requirements in wind turbine applications: 1) the current control time constant should be minimized and 2) active damping actions should effectively mitigate the LCL resonance. After the theoretical development, an insightful case study is provided. It is shown that the tuning problem can be solved approximately by root-loci inspection and an optimum solution can be found by direct search. The theoretical approach is experimentally verified by a lab-scale prototype that uses the same parameters of the case study.

Introduction

Grid-connected voltage source converters (VSC) usually work in current control mode: the PWM voltage reference is obtained from the current error in a closed loop. Current control mode of operation is common to most industrial application, as it provides features such as peak current control and disturbance rejection. In specific applications such as type IV wind turbines (full converter topology), the current controllers have a key role in the performance of the electric power conversion stage, as they are the innermost loops of a cascaded control structure [1–4]. In a cascaded loops structure, a suitable design guideline points to minimize the time constant of the innermost controllers [2–6]. Fast dynamics is also demanded to fulfill stringent grid-code requirements in faulty/weak grid situation [1–3].

On the other hand, LCL output filter configuration is employed in order to improve the filtering of switching harmonics and fulfil harmonic standards [7]. The selection of filter parameters is not a trivial task, as the internal resonance affects to the current controller dynamics [8]. Active and passive damping techniques have been proposed for a better dynamic behavior: the goal is to mitigate the harmonic amplification effects around the resonance frequency. In principle, passive damping is unwanted as it is associated to an efficiency loss [9]. Active damping techniques, on the contrary, mitigate the effects of the LCL resonance by proper control actions [8, 10–15]. The use of a filtered voltage feed-forward (i.e., use the capacitor voltage in an innermost loop) for active damping [8, 10, 13, 15] can be considered a convenient solution for wind turbine applications, because its simplicity and readiness (i.e., little modifications to the control structure, no extra sensors needed). Therefore, this technique has been considered in this work.

The main objective of this paper is to provide a systematic design approach, which addresses the specific control objectives (e.g., minimizing the dominant time constant) from a constrained system definition

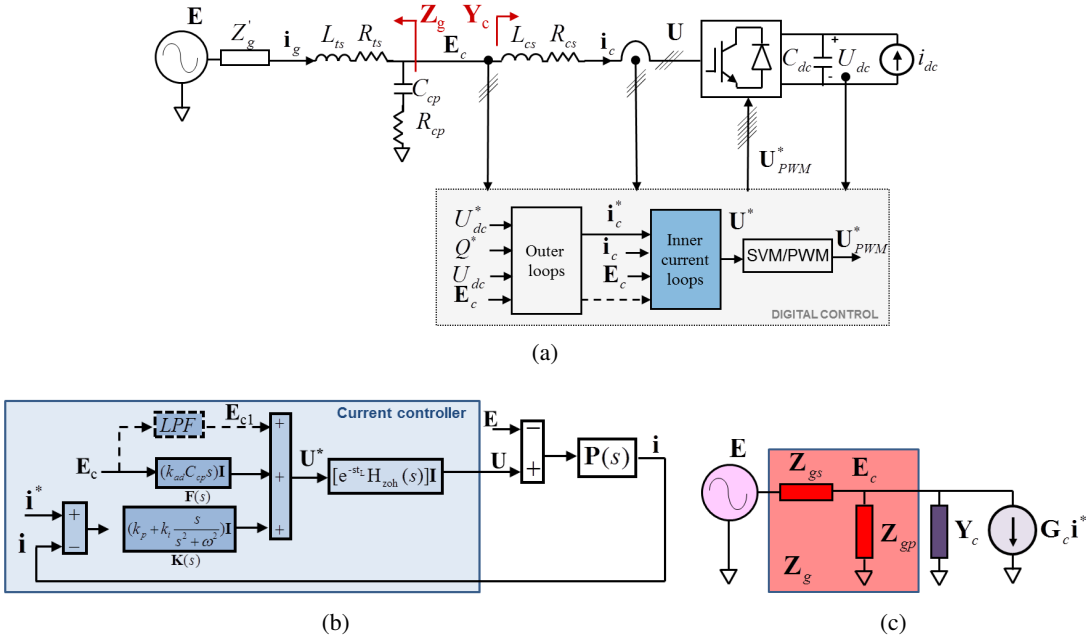

Fig. 1: System description. (a) LCL grid-connected VSC converter. (b) Current controller. (c) Admittance/Impedance formulation for dynamics assessment.

(e.g., in wind turbine applications, the hardware design is mainly imposed by the transformer leakage [7]). The impedance/admittance stability criterion [16, 17] is used to formulate the control problem: the converter dynamics are expressed by an equivalent converter admittance; the LCL capacitance branch in combination with the transformer leakage set the grid impedance [10, 13, 17]. Subsequently, from this formulation an equivalent nominal sensitivity transfer function is provided. It is shown as the root-locus of this equivalent nominal sensitivity describe the dynamics of the closed-loop system. Then, from a parametric analysis, it is possible to select the main control and active damping parameters to fulfill the control objectives: 1) maximizing the dominant time constant and 2) minimize harmonic interactions around the resonance frequency. Both objectives can be described analytically by the position of the dominant poles [4]. Therefore, an optimal solution to the tuning problem is obtained by a direct search that maximizes the absolute value of the dominant poles real part .

A lab-scale case study, which includes modelling, key diagrams and implementation details is provided. The experimental results prove that the high accuracy of the proposed methodology.

System Description and Modelling

Circuit Modelling

Fig. 1a represents a LCL grid-connected VSC working in current control mode. The voltages E, E_c and U represent the stiff grid, point of connection and VSC voltages, respectively. The LCL output filter is formed by the converter side inductive filter, the capacitance and transformer leakage model. The converter side inductive filter is defined by series inductance L_{cs} and resistance R_{cs}. The capacitance is given by a parallel capacitance C_{cp} in series with a small equivalent series resistor R_{cp}. The transformer model is given by a leakage inductance L_{ts} and a leakage resistor R_{ts} in series. The grid impedance is represented by $Z_g^{'}$, which depends on power system circuit and grid conditions [14, 18].

Focusing on a type IV wind turbine application, the biggest constraint in the hardware design is imposed by the transformer short-circuit current, which sets L_{ts}. Typical values for the secondary inductance are then in the range $[0.06, 0.1]$ p.u. of the machine rate power [7]. Following LCL design basic guidelines, the secondary inductance also constraints the selection of the converter filter: a primary inductance equal to the transformer inductance is a reasonable design both in terms of cost and dc-bus usage [7, 8]. Using

L_{ts} as a constraint (which may include the inductive part of $Z_g'(s)$ if available [7]), in practice, the main degree of freedom of the LCL filter is the choice of the capacitance C_{cp}. The LCL resonance frequency (angular) is given by

$$\omega_{res} = \sqrt{\frac{L_{cs}+L_{gs}}{L_{cs}L_{gs}C_{cp}}}. \tag{1}$$

The selection of ω_{res} involves a trade-off between control interactions and enhanced filtering [8, 9, 19]. From the point of view of the capacitor based active damping typical values at which the technique is more effective are in the range of $[0.1, 0.2]\omega_s$, with ω_s being the angular sampling frequency [8].

The role of the resistive components in the control problem is also important. From the VSC efficiency perspective, these are associated to system power losses. However, from the control point of view they have associated the positive effect of damping system responses [8, 9].

Current Controller Structure

Fig. 1b shows the analyzed controller structure. $K(s)$ represents the main controller, which in this work is a PR implemented in αβ-frame

$$\mathbf{K}(s) = (k_p + k_i \frac{s}{s^2+\omega^2})\mathbf{I} \tag{2}$$

with k_p and k_i being the proportional and resonant gains, respectively. $\mathbf{I}$ represents a 2x2 unity matrix, that means that $\mathbf{K}(s)$ is diagonal.

The control action calculation also includes an E_c voltage feedforward double path, with the following objectives: 1) provide a filtered value of the main grid component to improve the initial transient [20] and 2) an active damping action based on capacitor voltage derivative term [8, 13, 15]; the active damping action is given by

$$\mathbf{F}(s) = (k_{ad}C_{cp}s)\mathbf{I} \tag{3}$$

with k_{ad} being the active damping gain (C_{cp} is the capacitor nominal value). $\mathbf{F}(s)$ is also diagonal.

The system delay is modelled by a time latency t_L due to discrete-time operation (e.g., A/D and D/A conversion times of the digital board) and half a control sample due to PWM [zero order hold (ZOH)] operation [3, 4, 13]. Even both blocks are usually merged in one pure delay one, it has been found that splitting the delay model in two transfer functions better matches the whole frequency response around ω_{res}.

The system plant is represented by $P(s)$, which is a function of the LCL filter components [and $Z_g'(s)$] [8, 11, 12].

The matrix notation in the figure represents the three-phase and scalar variables of the real circuit. Subsequently, for the sake of generality scalar notation is used, since no couplings between phases are considered.

Admittance/Impedance formulation for dynamics assessment of grid-connected VSCs

Fig. 1c shows an alternative formulation of the grid-connected current controlled VSC problem. The converter controller and main filter, which are well parametrized during the design stage, are modeled by an equivalent admittance $Y_c(s)$ [and the closed loop gain $G_c(s)$ which sets the dependence on the current reference]. The converter dynamics are set by the admittance interacting with the rest of grid impedances, grouped in $Z_g(s)$; i.e., the $Y_c(s)Z_g(s)$ Nyquist trajectories set the dynamics of the system [13, 17, 21, 22].

In the context of the analyzed problem, a key feature of the Impedance/Admittance formulation is that $Y_c(s)$ definition includes all the $E_c(s)$ internal feedback paths, which eases the study of active damping [10, 13].The explicit derivations of $Y_c(s)$ and $Z_g(s)$ are given in the following.

Table I: Physical System Parameters

Parameter	Value
Rated Power	$S = 2.2\,\text{kVA}$
Rated Voltage (Line to line RMS)	$V = 220\,\text{V}$
Sampling (and PWM switching) frequency	$f_s = 10\,\text{kHz}$ ($\omega_s = 2\pi f_s$)
Converter inductance	$L_{cs} = 8.6\,\text{mH}(0.123\,\text{p.u.})$
Converter equivalent resistance	$R_{cs} = 0.27\,\Omega(0.012\,\text{p.u.})$
Capacitor	$C_{cp} = 4.5\,\text{uF}(0.039\,\text{p.u.})$
Capacitor ESR	$R_{cp} = 1\,\text{m}\Omega(< 0.001\,\text{p.u.})$
Grid Side Inductance	$L_{gs} = 4.7\,\text{mH}(\text{trafo leakage}) + 1.8\,\text{mH} = 6.8\,\text{mH}(0.097\,\text{p.u.})$
Grid Side Resistor	$R_{gs} = 0.22\,\Omega(0.010\,\text{p.u.})$
LCL resonance frequency	$f_{res} = \omega_{res}/2\pi = 1.233\,\text{kHz}$
Latency (1 sample in dSpace DS1006)	$t_L = 1/f_s = 100\,\mu\text{s}$
PWM/ZOH delay	$t_{pwm} = 0.5/f_s = 50\,\mu\text{s}$

From Fig. 1a, the converter admittance transfer function is defined by the ratio $i_c(s)$ over $E_c(s)$, with $E_c(s)$ being defined as an ideal voltage source and the current reference set to zero [the closed loop gain $G_c(s)$ can be defined in a similar manner], i.e.,

$$Y_c(s) = \left.\frac{i_c(s)}{E_c(s)}\right]_{i_c^*=0} \quad \left(G_c(s) = \left.\frac{i_c(s)}{i_c^*(s)}\right]_{E_c=0}\right). \tag{4}$$

Using both circuit and (inner current) control equations [23], the following expression is obtained

$$Y_c(s) = \frac{1 - F(s)\, e^{-s/f_s} H_{\text{zoh}}(s)}{L_{cs}s + R_{cs} + K(s)\, e^{-s/f_s} H_{\text{zoh}}(s)} \tag{5}$$

It should be remarked that $Y_c(s)$ is a function of the interface filter in combination with the controller (including system delays) transfer functions. The effect of outer loops, such as phase-locked loop, dc-link or reactive power control, in $Y_c(s)$ can be neglected as in practice the bandwidth of those outer loops should be much smaller than ω_{res} [21–24]. Using a similar reasoning, the feedforward path filtering E_{c1} from E_c to improve the grid-connection initial transient [see Fig. 1b] can be also neglected [20].

On the other hand, the grid impedance as seen from the $E_c(s)$ point is given by the capacitance filter connected in parallel to the transformer leakage impedance.

$$Z_g(s) = Z_{gp}(s) /\!/ Z_{gs}(s) \tag{6}$$

$$Z_{gp}(s) = 1/(C_{cp}s) + R_{cp} \tag{7}$$

$$Z_{gs}(s) = L_{ts}s + R_{ts} + Z_g^{'}(s). \tag{8}$$

Root-Locus based Tuning Derived from the Impedance/Admittance Formulation

Starting from the Impedance/Admittance Stability formulation, a systematic methodology to calculate the root locus and then tune the current controller is developed in this section.

By assuming that both $Y_c(s)$ and $Z_g(s)$ are open loop stable[1], a modified sensitivity transfer function is defined as

$$S_m(s) = \frac{1}{1 + Y_c(s)Z_g(s)} \tag{9}$$

[1]This condition is imposed to avoid unstable pole-zero cancellations [25]. $Z_c(s)$ is stable by definition. $Y_c(s)$ stability can be checked in the design stage.

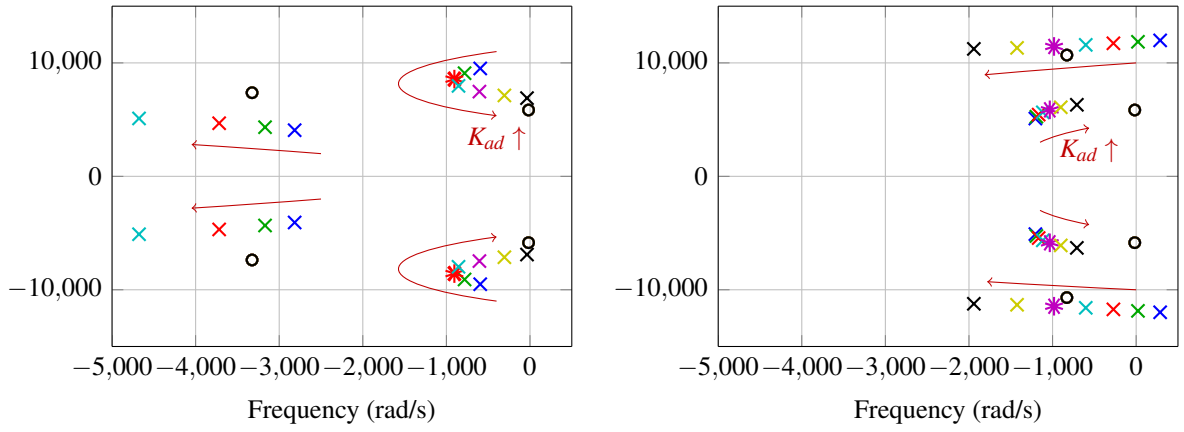

Fig. 2: (a) "Moderate α_c" tuning: root-locus by a k_{ad} sweep with $\alpha_c = 0.05\omega_s$; (b) "High α_c" tuning: root-locus by a k_{ad} sweep with $\alpha_c = 0.1\omega_s$.

Then, the dominant poles of the closed-loop system are available from the $S_m(s)$ root-locus.

In practice, since the LCL filter defines a poorly damped physical system, the dynamics are defined by an under-damped second order system. The dominant pair of poles is defined as $p_{d_{\pm j}}$. As shown below $\Im(p_{d_{\pm j}})$ is around $\pm\omega_{res}$, which provides physical meaning to the model: the roots associated to ω_{res} oscillations limit the dynamics of the system. Furthermore, since the system is poorly damped $|\Re(p_{d_{\pm j}})| < |\Im(p_{d_{\pm j}})|$ is also found in practice.

Control and Tuning Objectives

As said in the introduction, identification and minimization of the dominant time constants of inner loops is a key objective in cascade loops [5, 6], such as the power-train controller in wind turbines [1–3]. Root locus inspection has been proved as a suitable method for tuning current controllers since the modeling of delays results in complex expressions (difficult to deal with analytically) [2–4]. The use of Impedance/Admittance formulation together with an accurate modeling of delay effects, provides a systematic methodology that is straightforward for the tuning problem of LCL grid-connected converters, including the effect of active damping.

The tuning objective is then to find the collection of k_p, k_i and k_{ad} parameters that fulfills the application objectives:

1. In order to minimize the current controller dominant time constant, $\Re(p_{d_{\pm j}})$ should lie in the left half plane (LHP), as further as possible from the right half plane (RHP).

2. In order to reduce the harmonic amplification of components around ω_{res}, the damping factor of the dominant poles, defined as

$$\xi_d = \frac{|\Re(p_{d_{\pm j}})|}{\sqrt{\Re(p_{d_{\pm j}})^2 + \Im(p_{d_{\pm j}})^2}} \tag{10}$$

should be maximized.

In practice, by maximizing $|\Re p_{d_{\pm j}}|$ both objectives are fulfilled.

Case Study

The parameters of the lab-scale prototype, used for experimental verification, have been employed to develop the theoretical approaches in a case study. Table I shows the physical parameters employed for

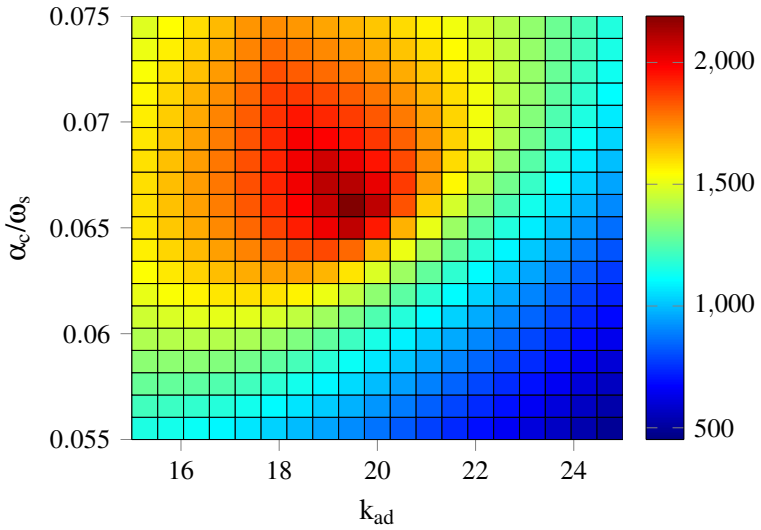

Fig. 3: Surface plot showing the results of the direct search in the $\alpha_c - k_{ad}$ axes. The gradient colors represent $|\Re(p_{d_{\pm j}})|$. The optimal solution (i.e., "optimal" tuning) is identified at $(\alpha_c = 0.066\omega_s, k_{ad} = 19.5)$.

analysis and experimental verification. It should be noted that $Z_g^{'}(s)$ is neglected in the analysis, since $|Z_g^{'}(s)| << |L_{ts}s + R_{ts}|$ is an accurate assumption for low-power scale circuits (i.e., the leakage inductor of a low power transformer is much higher than other impedances in the path of the stiff grid).

Different methodologies to get the tunings that fulfill the application objectives have been performed as explained below.

Tuning by Inspection

A criterion to start the tuning is first to consider that the dominant roots mainly depend on the proportional constant k_p [2, 3, 20]. The proportional constant is re-written as

$$k_p = (L_{sc} + L_{sg})\alpha_c \tag{11}$$

with α_c being the theoretical closed loop bandwidth [8, 13, 20]. The main reason to use this expression is to give physical insight to the k_p parameter [4, 20]. By means of a α_c (k_p) sweep (with $k_i = k_{ad} = 0$), it has been found that the real part of the dominant poles is maximized at $\alpha_c = 0.05\omega_s$. This gain can be considered a moderate one when compared to the maximum value defined by the one-to-tenth-rule, i.e., $0.1\omega_s$ [26]. Therefore, this tuning is named "moderate α_c".

Subsequently, the gain of k_i is introduced: a relatively low k_i does not give a significant change in the root locus; i.e.,

- the new roots result in pole-zero cancellations around $j\omega_1$ (resonant gains) so the system order is kept.
- The effect k_i on the main roots is relatively small; i.e., as expected k_p weights much more in the dominant poles placement.

It should be mentioned that, this reasoning applies in all the tunings; $k_i = 5000$ has been employed in all the root-loci (and in the experiments).

Subsequently, a k_{ad} sweep, which shown in Fig. 2a, seeks to identify the most convenient gain that maximizes the real magnitude of the dominant poles. The dominant poles that give the most convenient tuning (according to the proposed control objectives) are highlighted in red in Fig. 2a; the parameters are

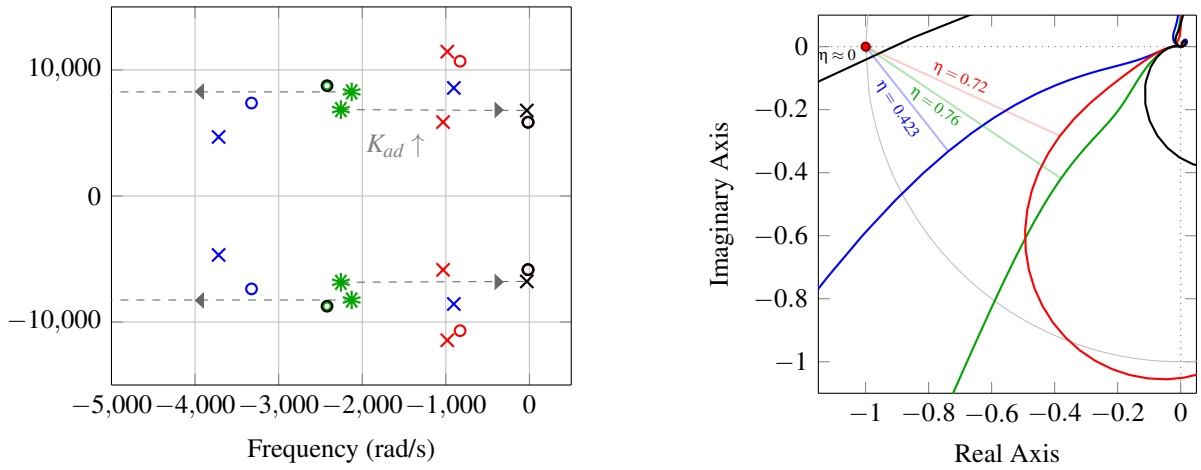

(a) (b)

Fig. 4: Comparison of tunings (a) Root-loci of the analyzed tunings: (blue) "moderate α_c"; (red) "high α_c"; (green) "optimum"; (black) "high k_{ad}". The dashed arrow represents the trajectories of the poles from the "optimal" tuning to "high k_{ad}" one as k_{ad} increases; (b) Nyquist trajectories corresponding to the analyzed tunings: (blue) "moderate α_c"; (red) "high α_c"; (green) "optimum"; (black) "high k_{ad}".

$\alpha_c = 0.05\omega_s$, $k_i = 5000$ and $k_{ad} = 10$. The dominant poles obtained with the "moderate α_c" tuning are $p_{d_{\pm j}} = -905 \pm 8570\,\text{rad/s}$.

Another criterion to start the tuning is by considering that the active damping is more effective changing the position of the dominant poles when the main controller has a high theoretical bandwidth [8]. This suggests that another tuning strategy starting from $\alpha_c = 0.1\omega_s$ (one-to-tenth rule [26]). Fig. 2b shows the root-locus based on a k_{ad} sweep for $\alpha_c = 0.1\omega_s$. This tuning is named "high α_c". It can be noticed that the system is unstable if active damping is not activated ($k_{ad} = 0$). With $k_{ad} = 20$ there is two sets of pair of poles with $\Re(p_{d_{\pm j}}) \approx -1000\,\text{rad/s}$ (i.e., a fourth order dominant response); in Fig. 2b, these roots are highlighted in purple .

Optimal Tuning

From the previous sections it can be seen that, overall, a moderate α_c is convenient to initially move the dominant poles to the left, but the tuning of k_{ad} is more effective for higher α_c values. Therefore, it is expected that there is an optimum set of (α_c, k_{ad}) values that places the dominant poles the furthest away from the RHP. This problem can be solved by finding the minimum of $\Re(p_{d_{\pm j}})$ [i.e., the maximum of $|\Re(p_{d_{\pm j}})|$ for stable solutions] in the (α_c, k_{ad}) plane, which has been solved by a direct search method [27]. Fig. 3 depicts $|\Re(p_{d_{\pm j}})|$ for a bounded set of (α_c, k_{ad}) that assures stability. The optimal solution is obtained with $\alpha_c = 0.066\omega_s$ and $k_{ad} = 19.5$, where $|\Re(p_{d_{\pm j}})| \approx 2150\,\text{rad/s}$.

Fig. 4a shows the different root-loci, including the "optimal" tuning (highlighted in green), which gives two set of dominant pair of poles with $|\Re(p_{d_{\pm j}})| \approx 2150\,\text{rad/s}$. A solution with $\alpha_c = 0.066\omega_s$ but high k_{ad} is also represented in order to show how a high k_{ad} drives the system to near to the RHP (instability). The latest tuning is named "high k_{ad}".

Correspondence with Nyquist Diagrams

Fig. 4b represents the Nyquist trajectories corresponding to the root-loci of Fig. 4a. Overall, it can be appreciated that the "moderate α_c", "high α_c" and "optimum" tunings provide low sensitivity peaks, defined by $1/\eta$ for each trajectory [5, 25, 28]. Low sensitivity peak means good relative stability; on the contrary, the "high k_{ad}" gives a high sensitivity peak; i.e., low conditional stability [5, 25, 28]. However, it can be appreciated the calculation of $p_{d_{\pm j}}$ is not so straightforward by inspection of the Nyquist trajectories [5].

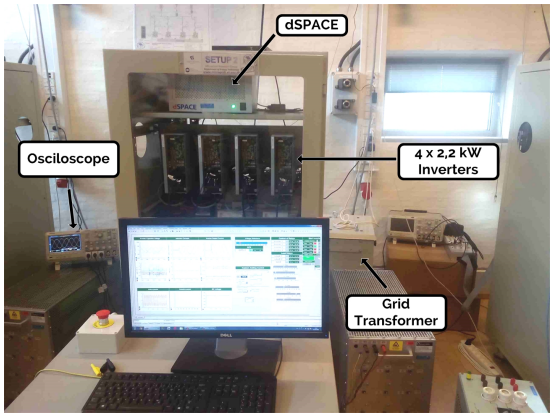

(a)

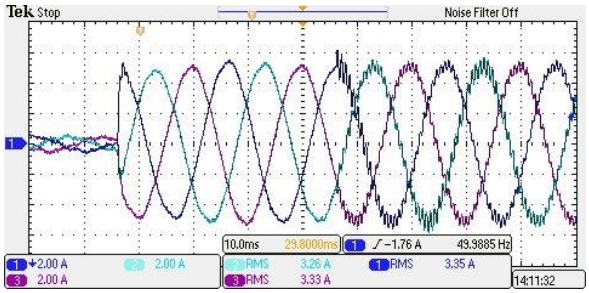

(b)

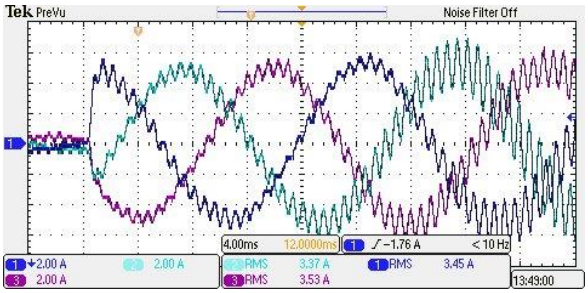

(c)

Fig. 5: Time domain results. (a) Experimental test-bed; (b) Active-current step at $k_{ad} = 19.5$ (convenient tuning) and then change to $k_{ad} = 35$; (c) Active-current step at $k_{ad} = 37$ (unstable system).

Experimental Results

Fig. 5a shows the test-bed used for the experimental verification. The main goal according to the application objectives, is to show that the optimum tuning provides a fast transient response together with a limited harmonic amplification in steady-state around ω_{res}. It is shown how this is achieved with the "optimal" tuning. Furthermore, when the dominant poles are moved towards the RHP (i.e., by means of increasing k_{ad}) the closed-loop performance is much worse both for transient and steady-state tests. This is shown by the "high k_{ad}" tuning.

Fig. 5b shows the grid current $i_g(t)$ during a step of amplitude $5A$ in the converter active current command (some reactive current flows the LCL capacitor when the converter current is zero). The system response is fast and tracks fast the reference. Then, after two cycles, k_{ad} is increased from 19.5 to 35. A steady-state oscillation of frequency $\approx \omega_{res}$ is identified, as expected from the "high k_{ad}" tuning that places dominant poles near the RHP.

Fig. 5c shows the star-up with $k_{ad} = 37$, which, from Fig. 4a suggest that the dominant poles enter on the RHP (i.e., higher k_{ad} than in the "high k_{ad}" tuning): as expected, the system is unstable, as accurately predicted.

Finally, the $i_g(t)$ harmonic spectrum for $k_{ad} = 19.5$ and $k_{ad} = 35$ are depicted in Figs. 6a and 6b. As expected, the system is better damped with $k_{ad} = 19.5$ (damping factor is close to zero when $k_{ad} = 35$), which is reflected with a lower amount of harmonics around the resonance frequency.

Overall, experimental results well match the predictions from the case study analysis and therefore, validate the theoretical approach.

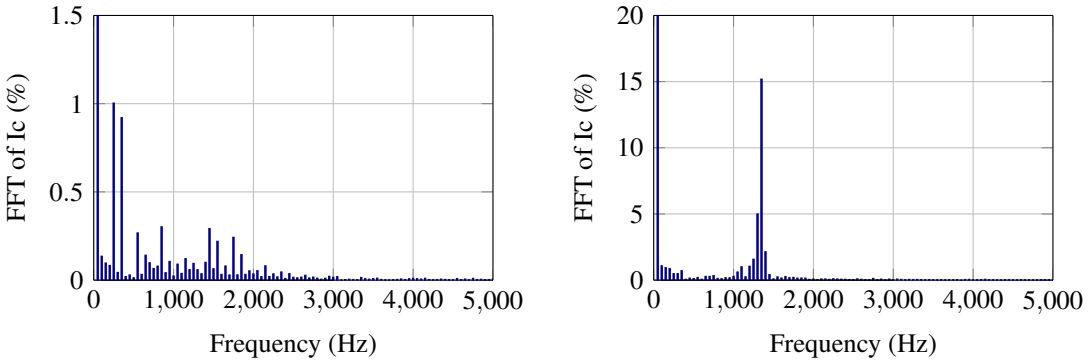

(a) (b)

Fig. 6: Harmonic spectrum with (a) $k_{ad} = 19.5$ ("optimal" tuning); (b) $k_{ad} = 35$ ("high k_{ad}" tuning) .

Conclusions

This paper contributes an original methodology for systematic design and analysis of current controllers with active damping for LCL grid-connected VSCs. The proposed design methodology is derived from the impedance stability criterion and is suitable for tuning according to objectives quantified in terms of 1) dominant time constant (i.e., the current controller is an inner loop of a cascaded system) and 2) damping factor of dominant poles (which have an imaginary part around ω_{res}). This control objectives explicitly focus on the Wind turbine applications, in which the grid VSC is connected through an LCL filter. The active damping method based on a capacitor voltage feedfoward is addressed because its good features for this application. The proposed methodology relies on the root-locus calculation obtained from a modified sensitivity $[S_m(s)]$ transfer function. By root-loci inspection an insightful tuning method is provided. Subsequently, an optimal solution [i.e., a set of (k_p, k_i, k_{ad})] is obtained by a direct search in which the real part of the dominant complex poles is minimized. From the theoretical case study, it is show how both k_p and k_{ad} have an important impact on the response and a convenient combination has been obtained. The experimental results validate the theoretical analysis of the case study: experimental figures show the accuracy of the method showing both transient (current steps) and steady-state (harmony spectrum analysis) responses.

References

[1] A. Timbus, M. Liserre, R. Teodorescu, P. Rodriguez, and F. Blaabjerg, "Evaluation of Current Controllers for Distributed Power Generation Systems," *IEEE Trans. Power Electron.*, vol. 24, no. 3, pp. 654–664, Mar. 2009.

[2] A. Vidal, F. D. Freijedo, A. G. Yepes, P. Fernandez-Comesana, J. Malvar, O. Lopez, and J. Doval-Gandoy, "Assessment and optimization of the transient response of proportional-resonant current controllers for distributed power generation systems," *IEEE Trans. Ind. Electron.*, vol. 60, no. 4, pp. 1367–1383, Apr. 2013.

[3] A. Vidal, F. D. Freijedo, A. G. Yepes, J. Malvar, O. Lopez, and J. Doval-Gandoy, "Transient response evaluation of stationary-frame resonant current controllers for grid-connected applications," *IET Power Electronics*, vol. 7, no. 7, pp. 1714–1724, 2014.

[4] F. D. Freijedo, A. Vidal, A. G. Yepes, J. M. Guerrero, O. Lopez, J. Malvar, and J. Doval-Gandoy, "Tuning of synchronous-frame pi current controllers in grid-connected converters operating at a low sampling rate by MIMO root locus," *IEEE Trans. Ind. Electron.*, vol. 62, no. 8, pp. 5006–5017, 2015.

[5] K. Astrom and T. Hagglund, *PID Controllers: Theory , Design and Tuning, Second Edition*. Instrument Society of America, 1995, pp. 274–279.

[6] F. Shinskey, B. Liptak, R. Bars, and J. Hetthessy, "2.6 Control Systems–Cascade Loops," in *Process Control and Optimization, Volume II*. ISA, Taylor Francis, 2006, pp. 148–156.

[7] G. Gohil, L. Bede, R. Teodorescu, T. Kerekes, and F. Blaabjerg, "Line filter design of parallel interleaved vscs for high-power wind energy conversion systems," *IEEE Trans. Power Electron.*, vol. 30, no. 12, pp. 6775–6790, 2015.

[8] J. Dannehl, F. Fuchs, S. Hansen, and P. Thogersen, "Investigation of active damping approaches for pi-based current control of grid-connected pulse width modulation converters with LCL filters," *IEEE Trans. Ind. Appl.*, vol. 46, no. 4, pp. 1509–1517, 2010.

[9] R. Pena-Alzola, M. Liserre, F. Blaabjerg, R. Sebastian, J. Dannehl, and F. Fuchs, "Analysis of the passive damping losses in LCL-filter-based grid converters," *IEEE Trans. Power Electron.*, vol. 28, no. 6, pp. 2642–2646, 2013.

[10] L. Harnefors, A. G. Yepes, A. Vidal, and J. Doval-Gandoy, "Passivity-based stabilization of resonant current controllers with consideration of time delay," *IEEE Trans. Power Electron.*, vol. 29, no. 12, pp. 6260–6263, 2014.

[11] R. Pena-Alzola, M. Liserre, F. Blaabjerg, M. Ordonez, and Y. Yang, "LCL-filter design for robust active damping in grid-connected converters," *IEEE Trans. Ind. Informat.*, vol. 10, no. 4, pp. 2192–2203, 2014.

[12] S. Parker, B. McGrath, and D. Holmes, "Regions of active damping control for LCL filters," *IEEE Trans. Ind. Appl.*, vol. 50, no. 1, pp. 424–432, 2014.

[13] L. Harnefors, A. G. Yepes, A. Vidal, and J. Doval-Gandoy, "Passivity-based controller design of grid-connected vscs for prevention of electrical resonance instability," *IEEE Trans. Ind. Electron.*, vol. 62, no. 2, pp. 702–710, 2015.

[14] D. Yang, X. Ruan, and H. Wu, "Impedance shaping of the grid-connected inverter with LCL filter to improve its adaptability to the weak grid condition," *IEEE Trans. Power Electron.*, vol. 29, no. 11, pp. 5795–5805, 2014.

[15] Z. Xin, P. Loh, X. Wang, F. Blaabjerg, and Y. Tang, "Highly accurate derivatives for LCl-filtered grid converter with capacitor voltage active damping," *IEEE Trans. Power Electron.*, vol. 31, no. 5, pp. 3612–3625, 2016.

[16] L. Harnefors, M. Bongiorno, and S. Lundberg, "Input-admittance calculation and shaping for controlled voltage-source converters," *IEEE Trans. Ind. Electron.*, vol. 54, no. 6, pp. 3323–3334, 2007.

[17] J. Sun, "Impedance-based stability criterion for grid-connected inverters," *IEEE Trans. Power Electron.*, vol. 26, no. 11, pp. 3075–3078, 2011.

[18] N. Strachan and D. Jovcic, "Stability of a variable-speed permanent magnet wind generator with weak AC grids," *IEEE Trans. Power Del.*, vol. 25, no. 4, pp. 2779–2788, 2010.

[19] J. Dannehl, M. Liserre, and F. Fuchs, "Filter-based active damping of voltage source converters with filter," *IEEE Trans. Ind. Electron.*, vol. 58, no. 8, pp. 3623–3633, 2011.

[20] L. Harnefors, L. Zhang, and M. Bongiorno, "Frequency-domain passivity-based current controller design," *IET Power Electron.*, vol. 1, no. 4, pp. 455–465, Dec. 2008.

[21] M. Cespedes and J. Sun, "Impedance modeling and analysis of grid-connected voltage-source converters," *IEEE Trans. Power Electron.*, vol. 29, no. 3, pp. 1254–1261, 2014.

[22] B. Wen, D. Dong, D. Boroyevich, R. Burgos, P. Mattavelli, and Z. Shen, "Impedance-based analysis of grid-synchronization stability for three-phase paralleled converters," *IEEE Trans. Power Electron.*, vol. 31, no. 1, pp. 26–38, 2016.

[23] L. Harnefors, "Modeling of three-phase dynamic systems using complex transfer functions and transfer matrices," *IEEE Trans. Ind. Electron.*, vol. 54, no. 4, pp. 2239–2248, Aug. 2007.

[24] B. Wen, D. Boroyevich, R. Burgos, P. Mattavelli, and Z. Shen, "Analysis of d-q small-signal impedance of grid-tied inverters," *IEEE Trans. Power Electron.*, vol. 31, no. 1, pp. 675–687, 2016.

[25] G. C. Goodwin, S. F. Graebe, and M. E. Salgado, *Control System Design*. Prentice Hall, 2000, pp. 80–81, 98–99, 178–189, 594–597, 603–608.

[26] S. Buso and P. Mattavelli, *Digital Control in Power Electronics*. Morgan and Claypool, 2006, pp. 25–30, 46–61, 93–98, 103–107.

[27] R. M. Lewis, V. Torczon, and M. W. Trosset, "Direct search methods: then and now," *Journal of computational and Applied Mathematics*, vol. 124, no. 1, pp. 191–207, 2000.

[28] A. Yepes, F. Freijedo, O. Lopez, and J. Doval-Gandoy, "Analysis and design of resonant current controllers for voltage source converters by means of nyquist diagrams and sensitivity function," *IEEE Trans. Ind. Electron.*, vol. 58, no. 11, pp. 5231 – 5250, 2011.